January – March 1993

ASAIO JOURNAL

Volume 39 • Number 1
ISSN 1058-2916

1058–2916/93/$3.00

ASAIO JOURNAL (ISSN 1058-2916) is published quarterly by the American Society for Artificial Internal Organs through J. B. Lippincott Company, 12107 Insurance Way, Hagerstown, MD 21740. Business offices are located at 227 East Washington Square, Philadelphia, PA 19106-3780. Printed in the USA. © Copyright 1993 by the American Society for Artificial Internal Organs, Inc. Second class postage paid at Hagerstown, Maryland, and at additional mailing offices. **Annual subscription rates:** United States, $160.00 individual, $220.00 institutional, $75.00 resident/student; all other countries except Japan, India, Nepal, Bangladesh, and Sri Lanka, $244.00 individual, $324.00 institutional. Single copies $80.00 (July/September issue, $160.00); Canada, $240.00 individual, $320.00 institutional. Rates for air mail delivery available upon request. Subscription rates in Japan: 52,000 yen individual, 68,000 yen institution (includes air mail postage). **Subscriptions, Orders, or Changes of Address** (*except Japan, India, Nepal, Bangladesh, and Sri Lanka*): Journal Fulfillment Department, J.B. Lippincott Company, 12107 Insurance Way, Hagerstown, MD 21740, or call 1-800-638-3030; in Maryland, call collect 301-714-2300. *In Japan,* USACO Corporation, 13-12, Shimbashi 1-chome, Minato-ku, Tokyo, 105 Japan. **Indexing:** ASAIO JOURNAL is indexed by *Chemical Abstracts* and *Index Medicus.* Sales Representative: Susan Eidson, Senior Accounts Manager, J.B. Lippincott Company, 227 East Washington Square, Philadelphia, PA 19106 (215) 238-4274. *MEMBERS' change of address:* American Society for Artificial Internal Organs, Inc., National Office, P.O. Box "C", Boca Raton, FL 33429. Copies will be replaced without charge if the publisher receives a request within 60 days of the mailing date in the U.S. or within 5 months in all other countries (Rates are subject to change).
POSTMASTER: Send address changes to ASAIO JOURNAL, P.O. Box 1550, Hagerstown, MD 21740.

Fluorescent Image Tracking Velocimetry of the Nimbus AxiPump

JOHN P. KERRIGAN,* FRANKLIN D. SHAFFER,† TIMOTHY R. MAHER,‡ TAMMY J. DENNIS,* HARVEY S. BOROVETZ,* AND JAMES F. ANTAKI*

High shear rates and extended residence times causing hemolysis and platelet activation can develop in an assist pump or cannula when inferior flow conditions exist. The high volume output of a miniature axial flow pump presents challenges in avoiding these adverse conditions. To assess the hemodynamics within the continuous flow Nimbus AxiPump, vector flow fields inside a translucent inflow cannula and a modified 12 mm AxiPump were mapped. Fluorescent image tracking velocimetry was used to track the motion of neutrally buoyant fluorescent particles (30 μm) using pulsed laser light, high resolution video cameras, and computer image analysis. An acrylic pump housing and cannula were integrated into a mock circulatory loop filled with a Newtonian, optically clear blood analog fluid. The flow parameters were controlled to yield known, physiologic loading conditions, including varying degrees of pulsatility. Cannula flow visualization results exhibited critical recirculation patterns at the bend. These results will be used to further optimize the design of the inflow. Particle impact was seen at the pump inlet in the inducer region of the rotor. Very good attachment of flow from the rotor to stator was observed when the pump operated at normal operating speeds. Intermittent regurgitant flow fields were evident in the presence of increased pulsatility and low pump speed. These results have lead to improvements in impeller design and speed control criteria to avoid potential deleterious flows. *ASAIO Journal* 1993; 39: M639–M643.

Visualization of the 12 mm Nimbus AxiPump[1] is performed to evaluate the fluid dynamics within the current design of the inflow cannula and pump chamber. The blood contacting portion of the Nimbus AxiPump consists of a rotor-stator body centered within a straight, rigid conduit. The rotor spins at 7,000 to 13,000 revolutions per minute (rpm), impartng kinetic energy to the fluid. The stator is a stationary region of the pump body that straightens the rotational flow produced by the rotor, thus recovering pressure head. Factors to be evaluated by the current set of experiments include an analysis of the fluid dynamics as the pump is subjected to a range of operating environments. These were selected to model conditions encountered in our *in vivo* studies.

Fluorescent image tracking velocimetry (FITV) is a noninvasive method of concurrently quantifying the trajectory of a two-dimensional flow field.[2] Our investigative approach qualitatively analyzes the flow conditions within the AxiPump and identifies suboptimal areas. This visual technique also supplements our understanding of how the microflow is affected by various conditions and control strategies.

Materials and Methods

A transparent (polymethylmethacrylate [PMMA]) model of the AxiPump cannula and housing was fitted with a cable driven rotor-stator assembly to provide optical access to the internal flow **(Figure 1).** A "U" shaped inflow cannula was used in this study to match the prototype used currently *in vivo*. A mock circulatory loop was configured and instrumented to maintain controllable preload and afterload con-

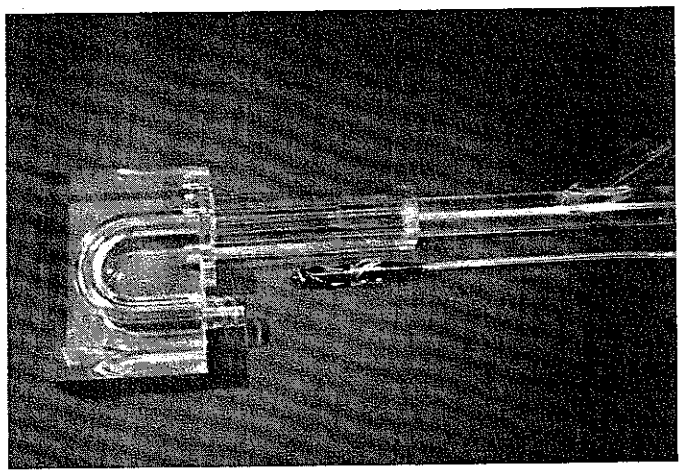

Figure 1. The disassembled transparent model of the inflow cannula and pump housing alongside the 12 mm cable driven model of the AxiPump. During visualization the pump was run at speeds from 7,000 to 13,000 rpm.

From *the Artificial Heart and Lung Program, University of Pittsburgh, Pittsburgh, Pennsylvania; †the United States Department of Energy, Pittsburgh, Pennsylvania, and ‡Nimbus, Incorporated, Rancho Cordova, California.

Reprint requests: John P. Kerrigan, C-811 Presbyterian University Hospital, Artificial Heart and Lung Program, University of Pittsburgh Medical Center, DeSoto @ O'Hara Streets, Pittsburgh, PA 15213.

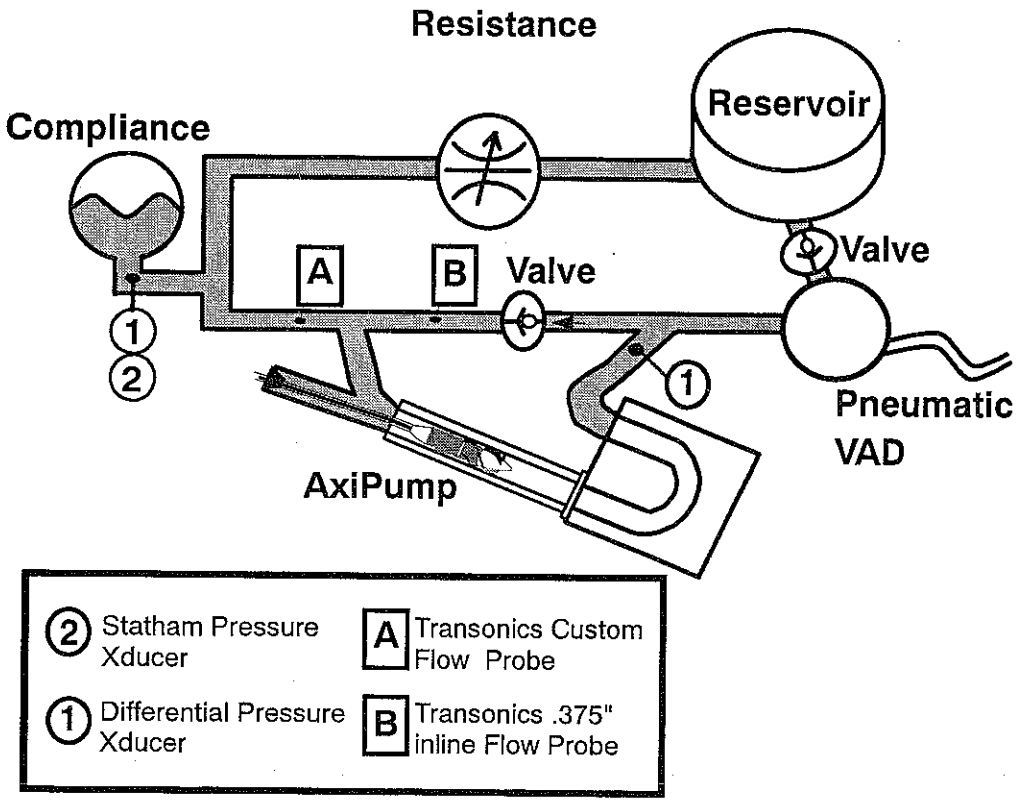

Figure 2. The instrumented circulatory loop used to model the cardiovascular conditions affecting the Nimbus AxiPump. The pump is in parallel with the modelled aortic valve. Afterload, pulsatility, and pump speed were the independent adjusted variables.

ditions to the pump **(Figure 2).** The loop consisted of a pneumatic ventricular assist device acting as the native left ventricle. Regulation of this VAD was accomplished by manually adjusting the drive pressure. The AxiPump was placed in parallel with a simulated aortic valve. A reservoir, compliance chamber, and pinch valve permitted atrial pressure, systemic compliance, and systemic afterload to be independently varied. Flow was measured with Transonics flow probes (Transonics, Ithaca, NY), and pressure was measured using Spectramed (Oxnard, CA) pressure transducers.

The viscosity of the blood analog solution, water-glycerol, was measured during all trials and maintained between 3.6 and 4.0 cps. Neutrally buoyant fluorescent particles, 30 μm in size (Duke Scientific, Palo Alto, CA), were slowly introduced into the fluid until the proper particle concentration was observed.

Details of the FITV set-up have been reported previously.[3] A 1 to 3 mm thick sheet of laser light emanating from a 5 watt Argon laser passes through the area of interest. The fluorescent particles are excited by the laser and, because of their inherent Stokes shift property, emit light at a longer wavelength. A Raman filter is placed between the field of view and the recording camera to virtually eliminate reflective glare of the excitation light. For qualitative video analysis, a Sony 3-CCD camera (Park Ridge, NJ) was used. Quantitative image tracking was accomplished by pulsing the laser light at a frequency of 3,333 Hz. Images are captured through a programmable video controller (ANDROX Corporation, Quincy, MA) and a video camera (Model 81, Dage MTI, Michigan City, IN). A SUN 670 workstation (Sun Microsystems, Mountain View, CA) processed the images using tracking software developed at the U.S. Department of Energy. Velocities were determined by grouping the appropriate particle trajectories and calculating the calibrated distances between the equally timed points.

Conditions involving both steady and pulsatile flow were

Table 1. Selected Operating Conditions of Pulsatile and Steady Flow

Operating Condition	Pump Speed (rpm)	Pulsatility	ΔP (mmHg)	Mean Flow (L/min)	Nondimensional Indices			
					π_1	π_2	π_3	N_s
1	7,000	—	15	1.9	9.4	48.0	0.45	0.17
2	11,000	—	85	1.5	4.7	20.8	0.10	0.22
3	13,000	—	75	4.0	10.7	14.9	0.16	0.43
4	10,000	High	63	1.6	5.6	24.7	0.14	0.21
5	10,000	Medium	32	3.1	10.8	24.0	0.26	0.30
6	12,000	Low	58	3.7	10.7	17.1	0.32	0.39

π_1, capacity coefficient; π_2, head coefficient; π_3, power coefficient; N_s, specific speed.

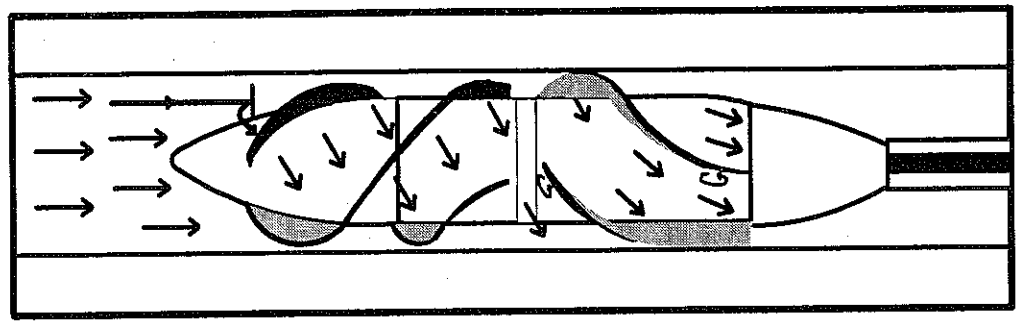

Figure 3. Flow patterns witnessed during steady flow with optimal pump speeds. Particle impact at the rotor entrance and two separation regions in the stator were the only perturbations from ideal flow visualization patterns.

qualitatively studied **(Table 1).** During steady flow experiments, the drive line of the pneumatic VAD was disconnected. The flow capacity of the cable-pump was regulated by altering the afterload. Increasing the systemic resistance increased the head (ΔP) across the pump, decreasing the capacity. H-Q plots graphically illustrating the AxiPump's characteristic flow map have been reported previously.[1] The systemic resistance value during the separate trials ranged from 0.4 mmHg/ml/sec to 4.0 mmHg/ml/sec. During pulsatile conditions, the drive pressure of the pneumatic VAD was adjusted between 80 and 150 mmHg; beat rate and systolic duration were kept constant at 70 bpm and 40%, respectively. The magnitude of pulsatility was defined by the ratio of the peak-to-peak flow ($Q_{p\text{-}p}$) and the mean flow (Q), and was classified as:

"highly pulsatile" if $Q <= 4\ Q_{p\text{-}p}$,
"moderately pulsatile" if $Q \approx Q_{p\text{-}p}$, and
"mildly pulsatile" if $Q > Q_{p\text{-}p}$.

Included in **Table 1** are the derived nondimensional indices for each of the conditions studied. Characteristic dimensionless groups are reported to ensure the kinematic and dynamic similarity between this model and the *in vivo* prototype.[4] The computed terms are the capacity coefficient (π_1) the head coefficient (π_2), the power coefficient (π_3), and the specific speed, N_s.

The flow within the pump was analyzed by considering three regions. Region A includes the rotor and extends 1 cm downstream from the rotor tip. Region B is defined as the transitional region between the rotor and stator. This region includes the initial attachment of the flow to the stator blade. Region C is the remaining area of the stator. The exiting flow from the pump could not be studied because of interference by the cable drive.

Results and Discussion

Steady Flow

A diagram illustrating the standard flow patterns witnessed during optimal pump speeds for the conditions tested is shown in **Figure 3.** Operating at properly controlled pump speeds for the modeled cardiovascular state, flow patterns at the inlet to the pump were laminar. Good attachment of the flow to the rotor nose was also evident. Particle impact at the rotor blade entrance was frequently observed, and this was attributed to the acute rotor blade angle at this portion of the impeller. Modifications to future designs have been made to correct this problem.

The angle of flow in region A was dependent on rotor speed. With higher rotor speed, and ensuing flow rate, the particle trajectories were more axial. Transition of the flow from the rotor to the stator showed good attachment and thorough washing of the convex (high pressure) side of the stator blade. Two small regions of flow separation on the concave (low pressure) side of the stator blades were evident, however. One region was located at the proximal edge of the blade and the other at the distal end. The magnitude of the separation was sensitive to the pump speed and systemic afterload. A higher pump speed created a broader separation region. Flow computations are underway that will optimize the shape of the stator blades to eliminate separation problems.

Recirculation regions on the inside curve of the U-shaped cannula were prominent. Secondary flow patterns in the plane normal to the flow also were recorded, and were consistent with previous observations.[5] As a result of these findings, alternative inflow cannula designs will be investigated.

Afterload and preload states influenced the flow patterns, depending upon the speed and head of pump operation.

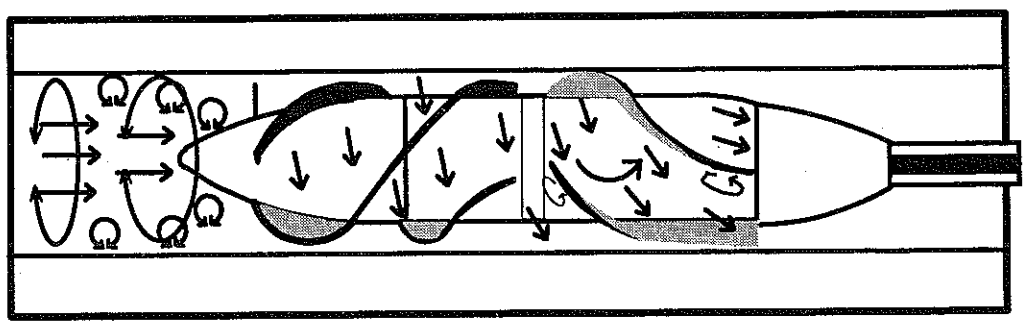

Figure 4. Flow patterns witnessed during highly pulsatile flow with suboptimal pump speed. This worst case condition resulted in high turbulence and swirl flow at the inlet, larger separation regions in the stator, and longer exposure times.

Table 2. Steady Flow Results

	Near-Surge (High Pressure/Low Flow)			Optimal Flow (Control)			Near-Stall (Low Pressure/ High Flow)		
	A	B	C	A	B	C	A	B	C
Flow phenomenon									
Turbulence	3	—	—	0	—	—	0	—	—
Recirculation/separation	3	2	3	0	1	2	0	2	2
Particle impact	2	3	0	2	3	0	3	2	0

Manifestation: 0, not seen; 1, transient; 2, consistent, minor; 3, prominent. Pump region: A, impeller inlet; B, transition region; C, stator.

Table 3. Pulsatile Flow Results

	High Pulsatility			Moderate Pulsatility			Low Pulsatility		
	A	B	C	A	B	C	A	B	C
Flow phenomenon									
Turbulence	3	—	—	1	—	—	1	—	—
Recirculation/separation	3	2	3	2	1	3	2	1	2
Particle impact	1	3	0	2	2	0	1	2	0

Manifestation: 0, not seen; 1, transient; 2, consistent, minor; 3, prominent. Pump region: A, impeller inlet; B, transition region; C, stator.

When the pump was operating at a high speed against a large afterload and low flow (near-surge), a large region of swirl and secondary flow was evident at the pump inlet. The direction of particle motion in the rotor became more circumferential during this near-surge state. As a result, the particles were exposed to higher shear for relatively longer periods than necessary. The particle direction as it exits the rotor maintains its circumferential direction, which exacerbates the separation regions at the low pressure edges of the stator **(Figure 4).**

When the pump was operating against a small afterload and high flows (near-stall), the flow patterns were similar to those in **Figure 3.** These results emphasize the importance of operating the pump outside the near-surge region. This will be incorporated as a consideration for future pump speed control algorithms. A qualitative summary of the steady flow results is listed in **Table 2.**

Pulsatile Flow

Table 3 summarizes flow properties in the AxiPump during three separate pulsatile conditions. Under high pulsatility states, the mean systemic pressure was approximately 150 mmHg with a range of over 60 mmHg. This placed extreme, time varying flow capacity requirements on the pump. Consequently, turbulence and recirculation were prominent at the pump inlet during ventricular diastole. Changes in the angle of flow inside the rotor were pronounced and dependent upon the phase of the cardiac cycle. The flow path was relatively axial during systole and circumferential during diastole. This caused the same inferior conditions that appeared during the near-surge steady flow state.

The area affected by disturbed flow at the pump inlet decreased as the magnitude of pulsatility decreased. An optimally controlled pump maintained good flow patterns at the medium and low pulsatile settings, with minor swirl flow at the inlet to the pump. The attachment of the flow from the rotor to stator produced sufficient washing of the stator blades. Minor areas of separation were evident at the concave side of the stator blades close to the transition region and at the pump exit as seen in the steady flow experiments.

The dynamic effects of pulsatile flow reduced the range of optimal pump operation in those cardiovascular states tested. Increased pulsatility produced greater ranges of flow demand on the pump. Under high pulsatility, this could effectively cause the pump to operate dynamically along its entire H-Q curve during a single cardiac cycle.

Conclusion

This study described microflow observations within the Nimbus AxiPump. The results have suggested design modifications to optimize hemodynamics within the pump and inflow cannula, which will be incorporated into the next generation system. Effects of pump control on flow also have been illustrated. It was evident that a healthy heart model is one of the most demanding environments in which to operate this pump with respect to flow. Further studies will visualize the newly designed version of the AxiPump and quantify flows in the various pump regions.

Acknowledgment

The authors thank Bill and Sue McGowan for their contribution to the University of Pittsburgh Artificial Heart and Lung Program. This project was supported by grant R44HL42701-02 from the National Institutes of Health.

References

1. Butler KC, Maher TR, Borovetz HS, et al.: Development of an axial flow blood pump LVAS. *Trans Am Soc Artif Intern Organs* 38: M296–M300, 1992.
2. Woodard JC, Shaffer FD, Schaub RD, Lund LW, Borovetz HS: Optimal management of a ventricular assist system. Contribution of flow visualization studies. *Trans Am Soc Artif Intern Organs* 38: M216–M219, 1992.
3. Shaffer F, Mathur M, Woodard J, et al.: Fluorescent image tracking velocimetry applied to the Novacor left ventricular assist device, in *Proceedings: ASME Fluids Engineering Conference*, Los Angeles, California, June 1992.
4. Ahmed N: *Fluid Mechanics*. San Jose, Engineering Press Inc., 1987.
5. Cheng KC, Inaba T, Akiyama M: Flow visualization studies of secondary flow patterns and centrifugal instability in curved circular and semicircular pipes, in Yang WJ (ed), *Flow Visualization III*, Washington, Hemisphere Publishing Corporation, 1983, pp. 531–536.